

Electrons and phonons in the ternary alloy $\text{CaAl}_{2-x}\text{Si}_x$ as a function of composition

Matteo Giantomassi,^{1,2*} and Lilia Boeri,³ and Giovanni B. Bachelet¹

¹*INFN Center for Statistical Mechanics and Complexity and Dipartimento di Fisica, Università di Roma "La Sapienza", Piazzale A. Moro 2, I-00185 Roma, Italy*

²*Istituto dei Sistemi Complessi, CNR, Via dei Taurini 19, 00185 Roma, Italy*

³*Max-Planck-Institut für Festkörperforschung, Heisenbergstr. 1, D-70569 Stuttgart, Germany*

(Dated: November 15, 2018)

We report a detailed first-principles study of the structural, electronic and vibrational properties of the superconducting C_{32} phase of the ternary alloy $\text{CaAl}_{2-x}\text{Si}_x$, both in the experimental range $0.6 \leq x \leq 1.2$, for which the alloy has been synthesised, and in the theoretical limits of high aluminium and high silicon concentration. Our results indicate that, in the experimental range, the dependence of the electronic bands on composition is well described by a rigid-band model, which breaks down outside this range. Such a breakdown, in the (theoretical) limit of high aluminium concentration, is connected to the appearance of vibrational instabilities, and results in important differences between CaAl_2 and MgB_2 . Unlike MgB_2 , the interlayer band and the out-of-plane phonons play a major role on the stability and superconductivity of CaAlSi and related C_{32} intermetallic compounds.

PACS numbers: 74.70.Dd, 71.15.Nc, 74.25.Kc, 74.25.Jb

INTRODUCTION

The discovery¹ of superconductivity at $T_c = 39$ K in magnesium diboride (MgB_2) is remarkable not only for its high critical temperature relative to conventional superconductors, but also because it has destroyed prejudices and created new hopes on electron-phonon (e-ph) superconductors. MgB_2 crystallises in the AlB_2 -type structure, also called C_{32} phase ($P6/mmm$, No.191),² forming hexagonal layers of graphene-like sheets of B atoms intercalated with Mg planes; the synthesis and study of materials with the AlB_2 structure has therefore attracted a great deal of interest in the last few years.

In the present paper we will focus on the ternary alloy $\text{CaAl}_{2-x}\text{Si}_x$, which has been recently synthesised³ for a relatively wide range of composition $0.6 \leq x \leq 1.2$ and, in this range, has been reported to be isostructural to MgB_2 , with honeycomb, graphene-like sheets of randomly distributed silicon and aluminium atoms, and alkaline-earth atoms intercalated between these sheets.³ Superconductivity has been detected in the whole composition range; the critical temperature $T_c(x)$ strongly depends on composition, showing a sharp peak at $x = 1$ (where $T_c = 7.8$ K), and dropping off rapidly as the Al/Si ratio departs from unity.³

Several experiments^{4,5,6} and *ab initio* calculations^{7,8,9,10} have concentrated on the $x = 1$ case (i.e. CaAlSi). Concerning the superconducting mechanism, Mazin *et al.*⁸ have suggested that the available experimental data could be reconciled with a traditional e-ph scenario, assuming the existence of a soft phonon mode ($\sim 30\text{-}40$ cm^{-1}); recently Huang *et al.*^{9,10} have calculated the phonon spectrum and electron-phonon coupling of CaAlSi , revealing the existence of a very soft (and, at some wavevector, even unstable) B_{1g} branch, which plays an important role in its superconducting properties; they also claim that this mode, which gets softer under pressure, can be invoked to explain the

positive pressure effect on T_c .¹⁰

In contrast to the $x = 1$ case, neither the wide stability range $0.6 \leq x \leq 1.2$ of the C_{32} phase, nor its instability outside this range (the limit of high aluminium or silicon concentration), nor any other physical property of $\text{CaAl}_{2-x}\text{Si}_x$ has been, so far, theoretically studied as a function of composition, at least to our knowledge.

Our paper reports the first detailed *ab initio* analysis of the structural, electronic and vibrational properties of this ternary alloy, both in the composition range for which it has been actually synthesised, and outside it, in the theoretical limits of high aluminium and high silicon concentration. The former limit ($x \rightarrow 0$) is of particular interest, since Ca and Al have the same valence configuration as Mg and B, respectively, and, therefore, the hypothetical¹¹ C_{32} phase of CaAl_2 would not only be isostructural, but also isoelectronic to MgB_2 , attracting attention as a possible new superconductor or, at least, as a relevant contribution to the understanding of MgB_2 and related superconducting alloys.¹⁵

The work is organised as follows. In Sec. I we briefly describe the computational details of our study, including the virtual crystal approximation adopted for a disordered alloy. In Sec. II we discuss the electronic bands of the $x=1$ case, considering both an ordered phase with in-plane Al-Si ordering and the disordered alloy, and compare our results with previous calculations^{8,9} and ARPES data.⁶ We also introduce a third, fictitious compound $\square^{2+}\text{AlSi}$, with calcium ions replaced by a uniform background of positive charge, whose electronic bands will help us identify the role of calcium ions. The vibrational properties and the electron-phonon coupling in CaAlSi and $\square^{2+}\text{AlSi}$ are presented in Sec. III while, in Sec. IV, we describe how the different Al/Si content modifies the electronic and structural properties of $\text{CaAl}_{2-x}\text{Si}_x$.

I. COMPUTATIONAL DETAILS

The electronic, structural and vibrational properties of all our crystals were calculated in the framework of the density functional theory^{16,17} and of the density functional perturbation theory¹⁸, with Kohn-Sham wavefunctions expanded on a plane-wave basis limited by a 40 Ryd cutoff energy.^{19,20} We used Troullier-Martins²¹ norm-conserving pseudopotentials generated by the FHI98PP package²² and consistently employed the GGA-PBE functional²³ to approximate the exchange-correlation energy functional. The \mathbf{k} -space integration (electrons) was approximated with a $12 \times 12 \times 12$ Monkhorst-Pack grid²⁴ for the self-consistent cycles; with the more accurate tetrahedron method²⁵ and a $20 \times 20 \times 20$ mesh for the electronic density of states (DOS); a $18 \times 18 \times 18$ Monkhorst-Pack grid for the electron-phonon coupling. After setting the smearing parameter²⁶ to 0.03 Ryd, the electronic total energies were converged to 0.1 mRy, while the phonon frequencies were converged within 5 cm^{-1} with respect to the \mathbf{k} -point sampling; we checked that a different choice of the smearing parameter between 0.02 Ryd and 0.04 Ryd would not change our frequencies by more than 5 cm^{-1} . Dynamical matrices were evaluated for phonon wave vectors \mathbf{q} on a $6 \times 6 \times 6$ grid, from which the phonon dispersion was obtained by Fourier interpolation.

To describe a disordered $\text{CaAl}_{2-x}\text{Si}_x$ alloy we employed the Virtual Crystal Approximation (VCA)²⁷, thus considering a $P6/mmm$ structure where the sites of the hexagonal graphene sheets are occupied by an alchemical element whose ionic pseudopotential is defined as $\hat{v}_{\text{ion}}^{\text{alch}} = (1 - x/2)\hat{v}_{\text{ion}}^{\text{Al}} + (x/2)\hat{v}_{\text{ion}}^{\text{Si}}$. The use of the VCA permits us to investigate the whole composition range $x \in [0, 2]$ without introducing superstructures (which on the other hand were not experimentally revealed in the samples examined with a powder x -ray diffraction technique).³ The VCA should be justified in our case, since Al and Si are neighbours in the periodic table and have a very similar electronic structure.

II. ELECTRONS IN CaAlSi , $\text{Ca}(\text{AlSi})$ AND $\square^2\text{AlSi}$

The $x = 1$ case requires a thorough discussion, since this is the composition to which most experimental and theoretical results refer. Furthermore, there is still an open question concerning the actual crystal structure, whether a chemically disordered phase (where each site of the hexagonal layers is randomly occupied by either Al or Si, with equal probability), or a crystal structure with some Al/Si ordering. The sharp x -ray diffraction patterns and the relatively high phase purity measured in CaAlSi (as opposed to the case of $\text{CaAl}_{2-x}\text{Si}_x$ with $x \neq 1$) suggest a possible Al/Si ordering for $x = 1$.³ This is also what Mazin *et al.*⁸ suggest, proposing a crystalline structure with atomic in-plane ordering (i.e., graphene-like sheets with alternated Al and Si atoms) of $P\bar{6}m2$ (No. 187) symmetry,² obviously lower than the C_{32} sym-

metry described above, and apparently favourable with respect to other possible ordering patterns.

An analysis of powder x -ray diffraction patterns performed by Imai *et al.*²⁸ suggests, instead, the disordered phase. The question is still under debate and no conclusive experimental measure has been reported yet.

To elucidate this controversy we have repeated Mazin's first-principles calculations, considering both the ordered $P\bar{6}m2$ structure and the disordered $P6/mmm$ VCA phase. Our comparison of these results with the ARPES experiments⁶ gives additional arguments in favour of the ordered phase. Moreover, the VCA phase represents a crucial reference for our subsequent rigid-band model. Hereafter we will indicate our disordered VCA phase as $\text{Ca}(\text{AlSi})$ and the ordered phase as CaAlSi . The CaAlSi and $\text{Ca}(\text{AlSi})$ lattice parameters were obtained by optimizing the structural parameters c and a up to a maximum residual stress of 1 MPa; the numerical values are listed in Table I.

TABLE I: Experimental lattice parameters at NTP³ and optimised lattice parameters for the ordered CaAlSi and the VCA-disordered $\text{Ca}(\text{AlSi})$ obtained in this work, based on GGA-PBE exchange-correlation and pseudopotentials.

	a (a.u.)	c (a.u.)	c/a
Exp	7.916	8.315	1.050
CaAlSi	7.979	8.446	1.058
% error	0.79	1.57	0.76
$\text{Ca}(\text{AlSi})$	7.965	8.485	1.065
% error	0.62	2.04	1.42

The agreement of the calculated lattice parameters with the experiment is good (slightly better for the ordered phase), with errors of the order of 1%. The corresponding electronic bands are shown in Fig. 1 for the ordered structure (upper panel) and the disordered VCA phase (middle panel); they agree quite well with the previous calculations,^{7,9} and, in particular, with the corresponding full-potential results⁸.

We will start our discussion with the energy bands of the ordered CaAlSi structure.

CaAlSi

In CaAlSi the sp^2 -hybrids of aluminium and silicon form three bonding σ bands: the lowest occupied σ band is formed by s -like states and is separated by a gap from the other two $\sigma(2p_{x,y})$ bands, which are mainly formed by the $2p_x, 2p_y$ states of Al and Si. The $\sigma(2p_{x,y})$ bands have

a quasi two-dimensional (2D) character, with a small dispersion along k_z (the Γ -A direction) very similar to what is observed in MgB_2 .^{29,30} We will refer to the $\sigma(2p_{x,y})$ bands as σ bands in what follows. The $2p_z$ states of Al and Si form a bonding (π) and an anti-bonding (π^*) band, which are completely three-dimensional (3D).

Because of the reduced crystal symmetry, the π and π^* bands do not cross at K , but are separated by a gap in the spectrum. And, unlike MgB_2 , both the bonding π and the bonding σ bands are fully occupied, because here there is one more electron per unit cell; so these bands cannot play any role for superconductivity. Moreover, because of the low c/a ratio, the π and π^* bands acquire a substantial dispersion along k_z , much higher than in graphite and MgB_2 ; the final result is that, in the ‘‘upper half’’ of the Brillouin zone ($k_z \simeq \pm\pi/c$, $A-L-H-A$ path), a good fraction of the π^* band is occupied too, and the antibonding π^* band, of 3D character, crosses the Fermi level.

Then, as we see in the upper panel of Fig. 1, a second band crosses the Fermi level. It’s a 3D band whose wavefunctions extend in the interlayer region. Its bottom has a prevailing $\text{Ca}3d_{z^2-r^2}$ character, yet the band as a whole may be easily traced back to the so-called graphite *interlayer band*,³¹ therefore, in what follows, we will stick to the name. This band is empty in graphite and MgB_2 , but here, in CaAlSi , it’s partially full, because of the different electron count.

As we see in the upper panel of Fig. 2, the CaAlSi Fermi surface resulting from these two bands has two topologically disconnected sheets. The first, outer sheet is a sixfold gear-like surface: a wide empty cylinder, whose axis is along k_z , connected to the neighbouring Brillouin zones in the k_{xy} plane along the Γ -M and equivalent directions by six sleeves, stretching out from its side surface. This sheet of the Fermi surface actually derives from both bands: near $k_z=0$ its character is mainly interlayer; near $k_z=\pm\pi/c$ it is mainly π^* . The second, inner sheet is a hexagonal lens-like structure centered at Γ . It exclusively arises from the interlayer band, which cuts ϵ_F (upper panel of Fig. 1) around the centre of the Brillouin zone (BZ). This structure is also observed in the ARPES data,⁶ which have revealed the presence of occupied states around Γ forming a hexagonal structure.

Ca(AlSi)

Comparing the $\text{Ca}(\text{AlSi})$ and CaAlSi bands of Fig. 1, we can notice that, because of the increased symmetry, the $\pi - \pi^*$ energy gap disappears in the VCA: now the π bands cross at K , forming an electronic pocket at E_F .

The most important difference is that the inner sheet of the Fermi surface, a large hexagonal lens in the ordered CaAlSi , shrinks to almost nothing in the VCA (a tiny circular lens, see lower panel of Fig. 2), because now the Fermi level cuts the interlayer band almost at its bottom, at Γ (see middle panel of Fig. 1). Otherwise, the

outer sheet is almost identical, differing from the corresponding one in CaAlSi only near the K point because of the additional small electronic pocket.

The lack of a sizable hexagonal lens-like structure makes the Fermi surface of the disordered structure less compatible with the experimental ARPES map. Furthermore, unlike the ordered phase, the band structure of the disordered $\text{Ca}(\text{AlSi})$ (middle panel of Fig. 1) cannot explain³² an ARPES high-intensity region located at ~ -0.8 eV, derived from π states, which is clearly visible in Fig. 2 of Ref. 6. Our results seem thus to confirm the existence of in-plane ordering in the compound synthesised with equal amounts of Al and Si.

While the bands of the ordered phase appear in better agreement with the ARPES experiment at $x=1$, the VCA band structure of the disordered $\text{Ca}(\text{AlSi})$, middle panel of Fig. 1, represents a very convenient reference for a rigid-band description of $\text{CaAl}_{2-x}\text{Si}_x$ at $x \neq 1$, a model which will prove quite accurate in the experimental range of compositions $x \in [0.6; 1.2]$. In a rigid-band framework we find it useful to report, on the right side of Fig. 1, the Integrated Density of States (IDOS), with black dashed lines corresponding to the band edges of the interlayer, σ , and π bands.

In this way we may see that, below 8.8 electrons, the π bonding band in the $k_z = 0$ begins to be emptied; below 8.5 electrons, the interlayer band is completely empty, and below 8.25 electrons the σ bonding band in the $k_z = \pm\pi/c$ plane begins to be emptied (see Section IV).

$\square^{2+}\text{AlSi}$

If a few differences in the electronic bands have helped us discriminate between the ordered and disordered phase, their similarity is overwhelming; the band structures in the upper and middle panels of Fig. 1 are, in fact, almost identical. Now we want to point out that the same striking similarity extends to the lower panel, where we show the bands of $\square^{2+}\text{AlSi}$. This fictitious compound has the same number of electrons and the same lattice parameters as CaAlSi , but the Ca^{2+} ion has been replaced by a homogeneous positive background \square^{2+} .

We see that the absence of the calcium ion doesn’t dramatically change the band dispersion at ϵ_F : the π^* is unchanged, while the interlayer band shows slight modifications. This indirectly confirms the interlayer character of this band. The important differences with respect to CaAlSi are located above ϵ_F , where the bunch of empty $\text{Ca}-d$ bands (and the corresponding large hump in the DOS) is clearly (and obviously) absent.

III. PHONONS AND E-PH COUPLING IN CaAlSi ($x = 1$)

Having become convinced that an atomic in-plane ordering takes place for $x = 1$, we will discuss the phonon

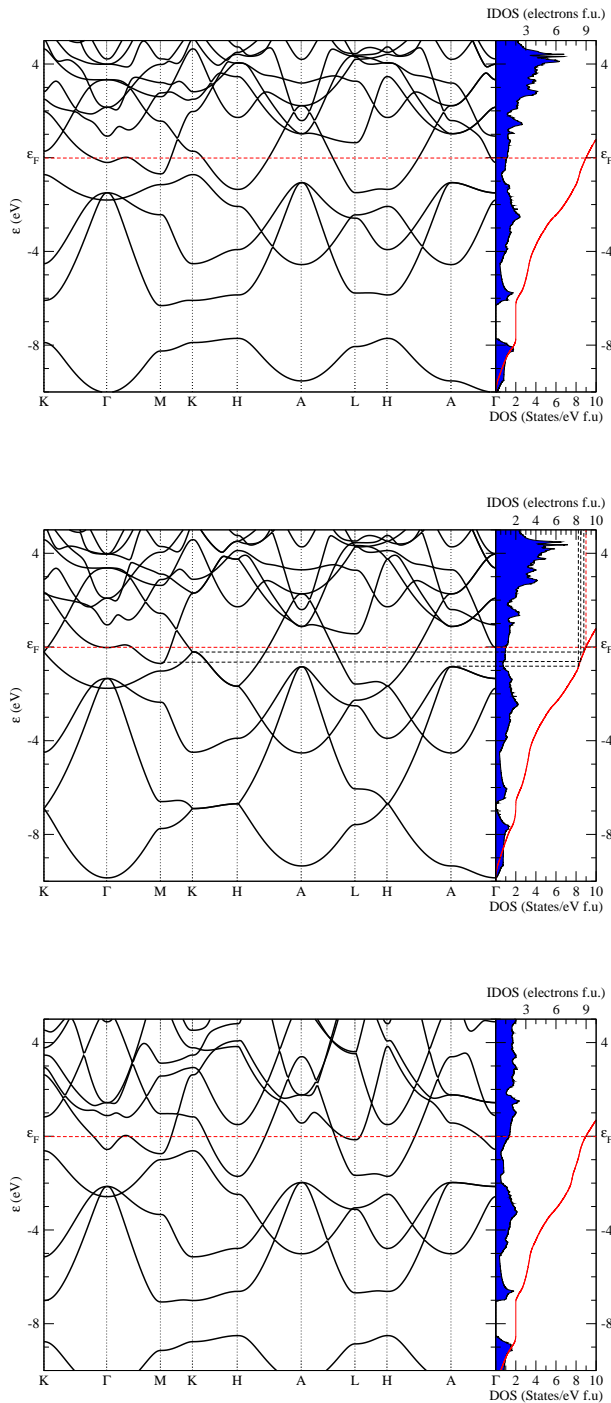


FIG. 1: Upper panel: energy bands (black), DOS (blue) and integrated DOS (IDOS, red) for CaAlSi. Middle panel: same as above for the disordered Ca(AlSi); the three black dashed lines pinpoint, along the IDOS, the number of electrons at which, in a rigid band scheme, a few relevant bands begin to be emptied or filled (see text). Lower panel: same as the upper panel, for the fictitious \square^{2+} AlSi.

dispersion only in the ordered phase, shown in the upper panel of Fig. 3. At the Γ point, in addition to the acousti-

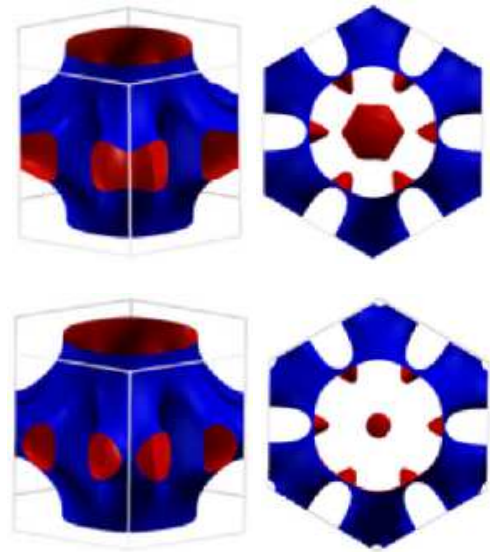


FIG. 2: Fermi surface and Brillouin zone of CaAlSi in the in-plane ordered (upper panels) and disordered (lower panels) structure. The outer sheet originates from both the π^* (around A) and the interlayer band (around Γ). The inner sheet (a lens-like structure) exclusively originates from the interlayer band at Γ , and is much larger, with more evident hexagonal symmetry, in the ordered structure (upper panel). We have chosen the blue color for the outer surface of the gear-like structure, and the red color for its inner surface. The surface of the inner, lens-like structure, is also red. With this choice the top view (right panels) happens to show the π^* part of the Fermi surface in blue and the interlayer part in red.

cal modes, there are four distinct optical modes: one doubly degenerate E_{1u} mode (vibrations of Ca atoms against the Al-Si planes along x, y), one A_{2u} mode (Ca vibrations against Al-Si planes along z), one doubly degenerate E_{2g} mode (in-plane Al-Si bond-stretching mode), and one B_{1g} mode (Al and Si displaced along z in opposite directions). Table II compares the frequencies ω of the optical modes at Γ obtained in this work with those reported in previous full-potential calculations. For comparison, in the same table we also report the corresponding phonon frequencies for MgB_2 ³³.

The most striking feature is the presence of a very soft B_{1g} mode. First intuition, inspired by the corresponding mode in MgB_2 and other diborides^{33,34}, would place this mode, which only involves vertical displacements of the lighter Al and Si atoms, at frequencies higher than those involving Ca too. We find it, instead, as the lowest-frequency optical mode not only at the Γ point (Table II), but also in the entire “upper half” of the BZ (Fig. 3). This finding can be reconciled with the mass argument only by a much weaker vertical force constant; and indeed, unlike the other compounds, CaAlSi has a partial filling of the π^* bands in the “upper half” of the Brillouin zone ($k_z \simeq \pm\pi/c$, $A-L-H-A$ path), which weakens

TABLE II: Calculated frequencies (cm^{-1}) of the zone-center optical phonons in ordered CaAlSi, as obtained here (asterisk) and in previous calculations. MgB_2 is shown for comparison.

	$B_{1g}(\Gamma)$	$E_{1u}(\Gamma)$	$A_{2u}(\Gamma)$	$E_{2g}(\Gamma)$
CaAlSi*	105	183	221	444
CaAlSi ⁹	99	194	222	455
CaAlSi ⁸	100	187	212	456
MgB_2 ³³	692	335	401	585

the bond in the vertical direction.

Our phonon frequencies at Γ (Table II) are in good agreement with all previous calculations; the same agreement is found with the entire phonon spectrum obtained by Huang *et al.*⁹, with a notable exception: our B_{1g} branch (upper panel of Fig. 3) has a frequency of $\sim 50 \text{ cm}^{-1}$ and is almost dispersionless in the $q_z = \pm\pi/c$ plane; Huang *et al.* find, instead, imaginary frequencies along the A-L path. We find no such dynamical instability either there, or, in fact, in any other phonon branch and wavevector. Our results agree with the overwhelming experimental evidence^{3,6,12} in favour of the structural stability of CaAlSi, and match the remarkable guess of Mazin *et al.*, that, outside Γ , a soft mode must be there at about $35\text{-}40 \text{ cm}^{-1}$ for a consistent explanation of both normal and superconducting properties.

In the upper panel of Fig. 3, right side, the calculated Eliashberg function $\alpha^2F(\omega)$, shown in red, is compared to the phonon DOS, shown in blue. The Eliashberg function evidently does not follow the phonon DOS, and shows a pronounced peak at $\sim 50 \text{ cm}^{-1}$, clearly arising from the (anomalously low) B_{1g} branch. Electrons mainly couple with this branch; the largest contribution to the integrated superconducting parameter λ will appear along the Γ -A-L path. This coupling is mainly interband in character: a B_{1g} displacement mixes the interlayer and π^* bands, while, by symmetry, the corresponding π - π coupling remains negligible^{35,36}.

Since, as discussed in Sec. II, Fermi-level interlayer electrons are near $k_z = 0$, while Fermi-level π^* electrons are near $k_z = \pm\pi/c$, the electron-phonon coupling happens at wavevectors in the “upper half” of the BZ ($q_z \simeq \pm\pi/c$, $A-L-H-A$ path). The total λ , obtained as a weighted sum over individual phonon linewidths, is 0.66. The critical temperature can then be estimated from the Dynes equation

$$T_c = \frac{\omega_{\log}}{1.2} \exp\left(-\frac{1.04(1+\lambda)}{\lambda - \mu^*(1-0.62\lambda)}\right); \quad (1)$$

with a calculated logarithmic average frequency of 151 K, and assuming $\mu^* = 0.1$, we obtain a T_c of 5.8 K, in reasonable agreement with the experimental T_c of 7.9 K.

In the lower panel of Fig. 3 we report the same vibrational properties (phonon dispersion, DOS and Eliashberg function) as in the upper panel, but calculated for the fictitious system $\square^{2+}\text{AlSi}$. Here we obviously have only 6 out of 9 phonon branches, since the Ca atoms are missing. Let us focus on the three optical modes, which correspond to the two E_{2g} branches (degenerate at Γ) and the B_{1g} branch of the original compound. Our results show that, while the two E_{2g} modes are more or less unchanged, the substitution of Ca ions with a uniform background of positive charge drives the B_{1g} branch towards imaginary frequencies (shown as negative in Fig. 3) across the entire Brillouin zone, indicating that our fictitious compound is not stable in this structure.

The Eliashberg function $\alpha^2F(\omega)$ (red line) is thus well defined for all branches except this one. At imaginary frequencies we may extend, as done here, its definition by taking their modulus. Such an extended Eliashberg function cannot be integrated to yield a total λ , but may be used to illustrate the frequency distribution of the e-ph interaction,³⁷ which turns out to be very similar to the real CaAlSi (upper panel). This is not surprising, because in $\square^{2+}\text{AlSi}$ the relevant, gear-like structure of the Fermi surface (not shown) is very similar to that of ordered and disordered CaAlSi (see Fig. 1). The only difference is that, in the fictitious $\square^{2+}\text{AlSi}$ (lower panel), the e-ph peak corresponding to the B_{1g} branch, is shifted to negative frequencies; we may therefore conclude that, although the Ca ion is not so important to define the CaAlSi electronic bands at ϵ_F , it plays a crucial role for its structural stability, because, with respect to the equivalent jellium-like charge, a positive ion placed between Al-Si layers is more effective both in binding them and in hindering the Al and Si vertical displacements.

In summary, we find an entire phonon branch of imaginary frequencies in the fictitious compound $\square^{2+}\text{AlSi}$, but we do not find any imaginary frequency in the phonon spectrum of the actual (ordered) CaAlSi, in contrast to previous, full-potential calculations. In CaAlSi we only find a very soft branch, which suggests the proximity of a structural transition. This single phonon mode, which is soft in the “upper half” of the Brillouin zone, dominates the electron-phonon coupling.

We suspect that a similar situation also holds at compositions other than $x=1$, and, in the following section, we explore in some detail the relation between lattice stability and band structure in the whole composition range. As we will see, the results confirm our hint, at least in the limit of high-aluminium concentration, and provide a useful reference and a strong motivation for a future, complete study of the electron-phonon interaction as a function of x .

IV. PHYSICAL PROPERTIES OF $\text{CaAl}_{2-x}\text{Si}_x$

In this section we will give a quantitative description and attempt a qualitative interpretation of how the com-

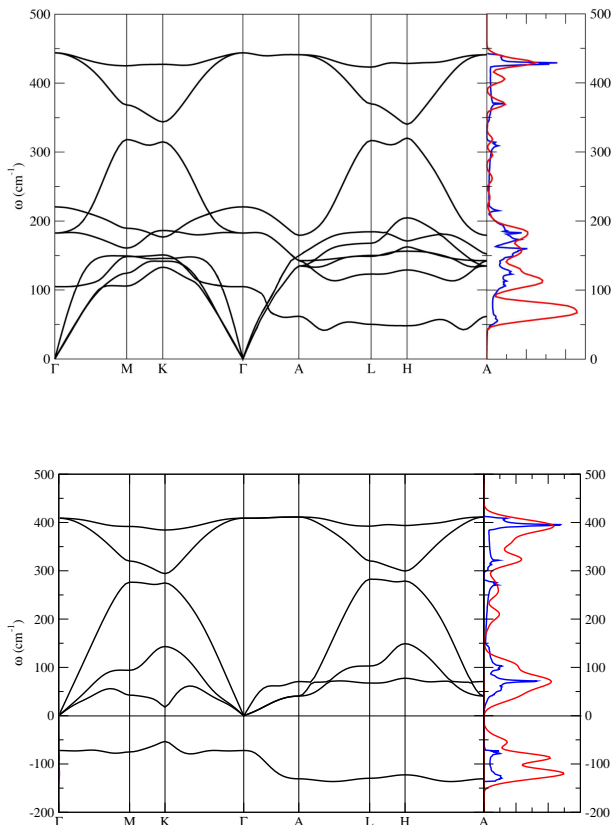


FIG. 3: Upper panel: Phonon dispersion, phonon DOS (blue) and Eliashberg function (red) $\alpha^2 F(\omega)$ for CaAlSi. Notice that the Eliashberg function has a large peak around 50 cm^{-1} , corresponding to the soft B_{1g} branch. Lower panel: same as above but in the fictitious $\square^2 \text{AlSi}$; the B_{1g} branch has an equally large e-ph coupling, but now its frequency are imaginary (negative in the plot) in the entire BZ, revealing a dynamical instability (see text).

position x affects the electronic and structural properties of the C_{32} phase of $\text{CaAl}_{2-x}\text{Si}_x$. We will consider a dense grid of x values in the range $[0, 2]$, which includes both the physical $[0.6, 1.2]$ and the unphysical range. For each x -value considered, the hexagonal unit cell has been optimised up to a residual stress of 1 MPa, and band structure calculations have been performed in the relaxed configuration. For this dense grid of x values a slightly lower cutoff of 36 Ryd was used for the plane-wave basis. In Fig. 6 we report, as a function of x , the optimised lattice parameters (upper panel) and $g(\epsilon_F)$, the calculated DOS at the Fermi level (lower panel, black). We start our discussion from the experimental x -range.

Experimental range, $0.6 \leq x \leq 1.2$

Taking into account that we have modelled the disorder using the VCA, and that the experiments detect several types of impurities, our theoretical in-plane bond

length appears in reasonable agreement with the experimental data; the largest discrepancies are observed close to $x = 0.6$, which is the lowest aluminium concentration for which the series has been synthesised. The somewhat worse agreement for c is common to the ordered phase and may be traced back to a systematic error of the approximate exchange-correlation functional.

In the whole experimental range, a monotonically decreases with x , while c is almost constant.

The small (less than 3%) variations in the lattice parameters correspond to minor modifications in the band structure: in the experimental x -range the calculated electronic structure of $\text{CaAl}_{2-x}\text{Si}_x$ (not shown) can be accurately described by a simple rigid-band model, where the Fermi level changes only according to the different number of electrons per cell $N_e(x) = 8 + x$, see Fig.1.

An indirect proof of the validity of this model is given in the lower panel of Fig. 6 where we plot, as a function of x , the self-consistent DOS at the Fermi level, $g(\epsilon_F)$, of $\text{CaAl}_{2-x}\text{Si}_x$ and the corresponding value for a rigid-band filling $N_e(x)$ of the (fixed) bands of $\text{Ca}(\text{AlSi})$, i.e., the bands shown in the middle panel of Fig.1. As we can see, in the composition range $0.6 \leq x \leq 1.2$, where the alloy is experimentally found to be stable in this crystalline structure, the two curves are almost identical; deviations start to appear at the extrema of this range. Then, outside this range, the rigid-band model completely breaks down. The dependence of $g(\epsilon_F)$ on composition thus correlates with rigid-band and structural properties. Its almost monotonic variation in the experimental range of stability $0.6 \leq x \leq 1.2$ does not, instead, correlate with the observed trend in the superconducting transition: the experimental $T_c(x)$ has a sharp peak at $x = 1$ and drops off rapidly as the Al/Si ratio is changed in either directions.³ This suggests, by exclusion, that the experimental trend in $T_c(x)$ must be associated with changes of the phonon frequencies and/or electron-phonon coupling strength as a function of composition.

High aluminium concentration, $x < 0.6$

For $x < 0.6$ the a lattice parameter still increases as x decreases, its slope being larger than in the experimental range of stability. Much more peculiar is the behaviour of the c parameter. Reverting the trend observed in the experimental range of stability, c decreases as x decreases, until it equals the a value, for $x \sim 0.3 - 0.4$; then, at $x = 0.2$, it undergoes an abrupt change, such that the c/a ratio jumps by $\sim 20\%$. Our lattice dynamical calculations show that this change is accompanied by the occurrence of dynamical instabilities.

In Fig. 4 we plot, as a function of x , the $\text{CaAl}_{2-x}\text{Si}_x$ phonon frequencies of the B_{1g} branch calculated at Γ , A and L (purely imaginary frequencies are shown as negative values). At $x < 0.2$ there is a large jump in the phonon frequencies of the B_{1g} branch at A and L, which become imaginary (shown as negative), while the zone-

center phonons are still all stable. The entire CaAl_2 ($x = 0$) phonon spectrum, shown in the lower panel of Fig. 7, reveals that the compound is dynamically unstable against lattice distortions with $q_z = \pm\pi/c$ and eigenvectors corresponding to the B_{1g} optical and A_{2u} acoustical branches, both implying an out-of-plane displacement of the Al - Si atoms.

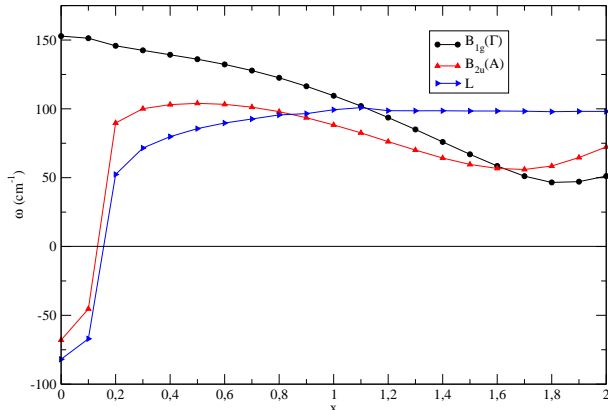


FIG. 4: Selected phonon frequencies of the spectrum of $\text{CaAl}_{2-x}\text{Si}_x$ as a function of the Silicon content x . The branch which corresponds to the out-of-phase displacement of the Al/Si sublattice along z (B_{1g} at Γ , B_{2u} at A) becomes unstable around $k_z = \pm\pi/c$ for $x < 0.2$ (imaginary frequencies are shown as negative).

The dramatic changes in the lattice parameters and phonon frequencies with compositions $x < 0.6$ can be rationalised in terms of the electronic band structure. We will start our discussion on the bands calculated at $x = 0.6$, shown in Fig. 5. At this composition both the interlayer band and the π bands cross the Fermi energy, while the σ bands are still completely full, even though, around A , they are now very close to ϵ_F . On these grounds one may think that, by further decreasing x (i.e., by increasing the aluminium content), it would be possible to obtain σ holes, as in MgB_2 . This simple hint proves, however, incorrect, since, as already mentioned (when discussing the lower panel of Fig. 6), the rigid band model breaks down for $x < 0.6$. We are going to make this statement more precise. Our first-principles calculations have revealed that the σ , π and interlayer bands are no longer rigid when the aluminium content is increased above 70% (i.e. for $x < 0.6$).

The π band decreases its binding energy on the $k_z=0$ plane, progressively losing electrons and getting emptier and emptier as x is reduced, while the interlayer and the σ bands remain partially filled to conserve the total number of electrons per unit cell; but then, as x further decreases, the crystal structure, and therefore the bands, substantially rearrange. In a rigid band picture, based on the $x = 1$ DOS, the interlayer band would become completely empty at $x=0.5$ (see middle panel of Fig.1);

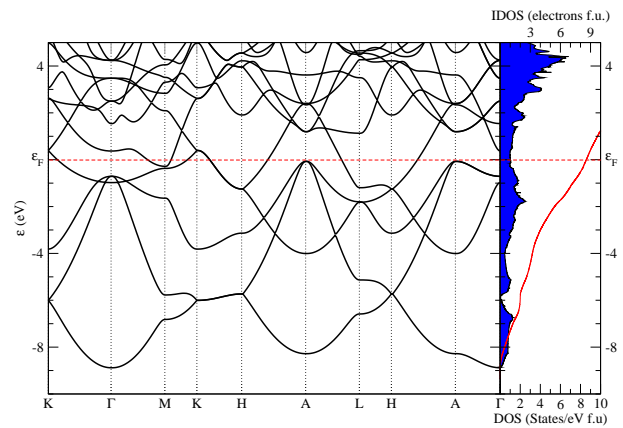


FIG. 5: Energy bands (black), electronic DOS (blue) and integrated DOS (solid red) at $x = 0.6$, i.e., the lowest Si concentration for which CaAlSi is observed in the C_{32} structure.

but, precisely around this composition, the rigid-band picture starts to break down, and the behaviour of the c/a ratio starts to change in such a way as to keep the interlayer band always at ϵ_F .

When, at $x = 0.2$, the interlayer band is almost empty, our self-consistent calculations predict a further, abrupt change in c/a . This sudden relaxation is related to a major rearrangement of all bands, whose main result is that the interlayer band stays at the Fermi level, while the π (bonding) band becomes completely empty in the $k_z=0$ plane.

The complete emptying of the π band in the “upper half” of the Brillouin zone ($k_z \simeq \pm\pi/c$, $A - L - H - A$ path) further weakens the bonds in the vertical direction, and this explains the appearance of imaginary frequencies in the out-of-plane phonon branches of the C_{32} phase of $\text{CaAl}_{2-x}\text{Si}_x$ for $x < 0.2$. The displacement corresponding to these phonons is compatible with the stable structure of CaAl_2 at ambient condition, the MgCu_2 Laves phase, in which the Al atoms sit on triangular layers intercalated by mixed Ca-Al planes. In this structure, the main bonding force is provided by $p-d$ bonds between Ca and Al, while in the C_{32} structure the in-plane sp^2 bonding is important. Interestingly, experiments have shown¹² that the Laves phase is stable only up to $x < 0.2$, where we find the occurrence of a lattice instability for the C_{32} phase. A thorough investigation of the whole phase diagram and transition goes, however, beyond the aim of the present study.³⁸

In the upper panel of Fig. 7 we display the electronic bands of CaAl_2 corresponding to the optimised C_{32} structure. Because of the large modifications in the lattice parameters, these bands bare very little resemblance to those of $\text{Ca}(\text{AlSi})$, and even less to those of MgB_2 . What seemed to be a good candidate for a compound with properties similar to MgB_2 turns out to be a very poor imitation, once the lattice parameters are optimised. In particular, even though there is a tiny amount of σ holes

around the A point –the fingerprint and main ingredient for superconductivity of MgB_2 –, in CaAl_2 most of the DOS at ϵ_F comes from the π^* bands and from the the interlayer band (which in MgB_2 is, instead, above ϵ_F , and thus completely empty). Worst of all, as we already saw, CaAl_2 is dynamically unstable in the C_{32} structure.

We wish to point out that the differences in the band structure and the dynamical instability are both a consequence of the c/a reduction: if we not only constrain the compound to the C_{32} structure, but also keep the c/a ratio at the same value as MgB_2 (rather than being optimised, as done until now), then we find σ holes at the Fermi level (see fig. 8) and a dynamically stable compound: all the calculated phonon frequencies, not shown, are now real.³⁹

We finally observe that the abrupt c/a reduction (when the crystal is, as in our calculations, artificially forced to maintain the C_{32} structure) amounts to a Fermi-level pinning of the bottom of the interlayer band. Since, as mentioned, the bottom of the interlayer band has a prevailing Ca- d character, this observation in turn suggests that the mechanism which makes CaAl_2 so different from MgB_2 and drives its instability towards the Laves phase is, in fact, the pinning at the Fermi level of the calcium d -states.

High silicon concentration, $x > 1.2$

While in the limit of high aluminium concentration ($x < 0.6$) we found several fingerprints and a plausible explanation for the experimental lattice instability, in the opposite limit (high silicon concentration, $x > 1.2$) the only remarkable finding remains the deviation from the rigid-band behaviour, which, as x increases, manifests itself in the slow descent in energy of the lowest anti-bonding σ band. This band, which at $x = 1$ is ~ 1 eV above E_F at Γ , starts filling up at $x = 1.6$.

Apart from this deviation (which however is less dramatic than for $x < 0.6$, see lower panel of Fig. 6), neither the optimised structural parameters a and c (upper panel of Fig. 6), nor the phonon frequencies selected in Fig. 4, nor, in fact, any frequency of the complete phonon spectrum (not shown), seem to do anything special in the composition range $1.2 \leq x \leq 2$. This suggests that (at zero temperature) the C_{32} phase of CaSi_2 (i.e., $x = 2$) represents a metastable structure, i.e., a local minimum of its total energy which is higher than the absolute minimum. Such a guess is reinforced by the complexity of the unit cells of the actual stable phases of CaSi_2 ⁴⁰, which could easily imply sizable energy barriers separating them from the metastable C_{32} phase.⁴¹

Again, a thorough investigation of the whole phase diagram and transitions of CaSi_2 goes beyond the aim of the present study.

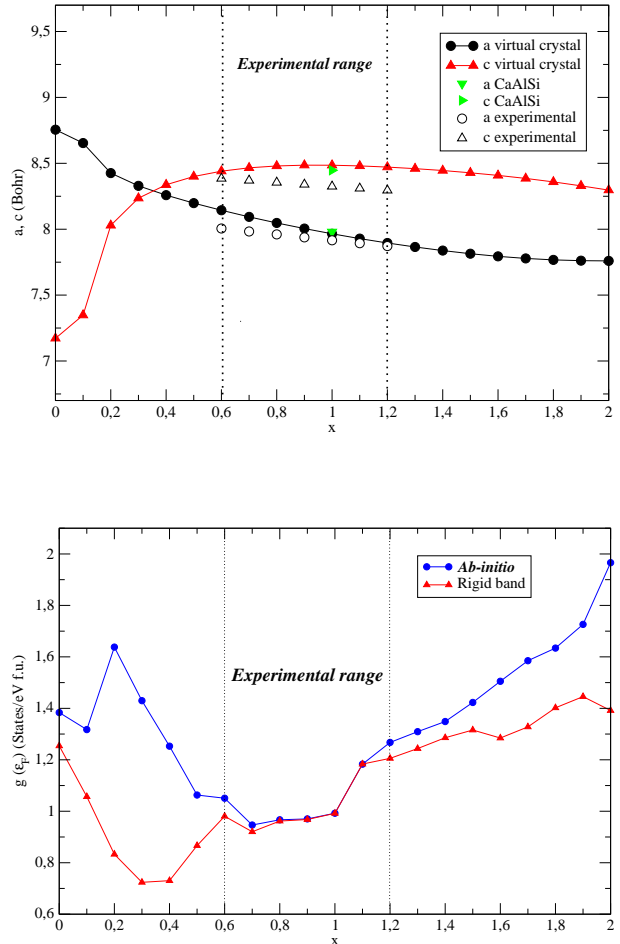


FIG. 6: Upper panel: optimised lattice parameters for the C_{32} crystalline structure of $\text{CaAl}_{2-x}\text{Si}_x$. Lower panel: blue circles indicate the self-consistent density of states at the Fermi level $g(\epsilon_F)$ of $\text{CaAl}_{2-x}\text{Si}_x$ in the fully relaxed structure, while red triangles show $g(\epsilon_F)$ obtained with a rigid-band filling of Ca(AlSi) appropriate to the electron number $N_e(x) = 8 + x$ (see middle panel of Fig. 1).

V. SUMMARY AND CONCLUSIONS

In this work we have reported first-principles calculations of the electronic and vibrational properties of the ternary alloy $\text{CaAl}_{2-x}\text{Si}_x$ in the entire composition range $0 \leq x \leq 2$, discussing how electronic, structural and vibrational properties are related to each other. In this context an interlayer band, which is empty in MgB_2 , and whose bottom has Ca- d character in our compounds, plays a major role.

At $x=1$ the electronic band dispersion and Fermi surfaces, calculated considering both an ordered phase with atomic in-plane ordering and a disordered VCA phase, confirms the suggestion of Mazin *et al.*⁸, that the com-

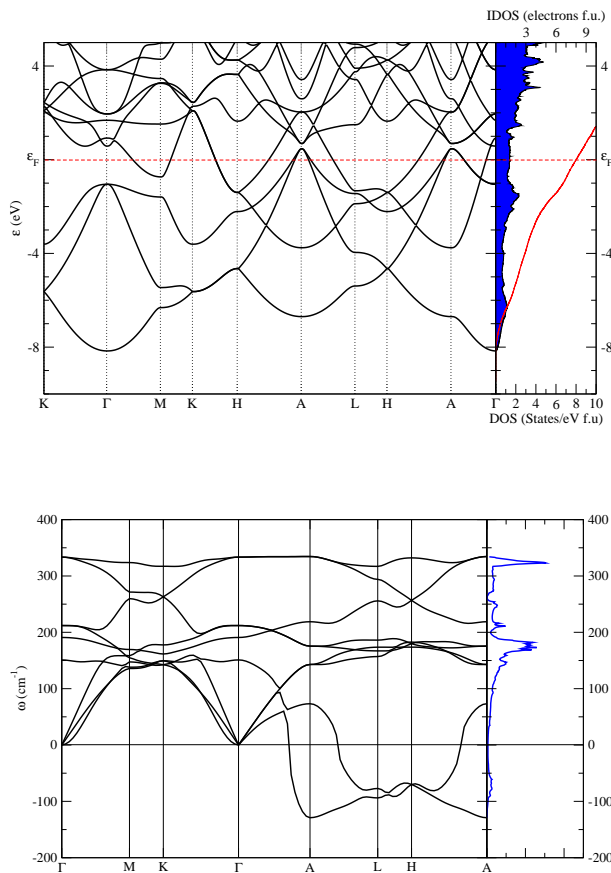


FIG. 7: Upper panel: energy bands and DOS for CaAl_2 in the structurally relaxed C_{32} structure. Because of the very small c/a , the π bands acquire a large dispersion in the k_z direction, and are driven well above ϵ_F in the $k_z=0$ plane. Notice that the resulting Fermi surface (not shown) is still similar to that of $\text{Ca}(\text{AlSi})$. Lower panel: phonon dispersion and density of states corresponding to the same structure.

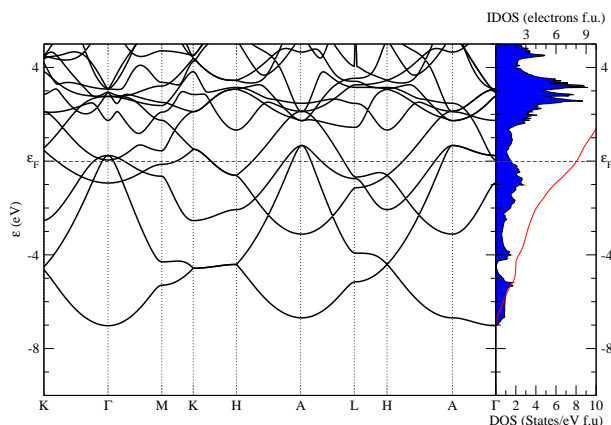


FIG. 8: Band structure of CaAl_2 in the C_{32} structure with the same c/a ratio as MgB_2 ($c/a=1.142$). In this case there are σ holes at the Fermi level both at A and Γ and all the phonon frequencies (not shown) are real.

pound crystallises in a completely in-plane ordered phase, if synthesised in presence of equal amounts of Al and Si. Our calculation of the electron-phonon coupling confirms that the soft B_{1g} phonon branch plays a major role in the superconductivity of CaAlSi , and shows that this mode couples the interlayer and π^* bands. At variance with a previous full-potential calculation, we do not find any instability in the phonon spectrum of CaAlSi .

At $x \neq 1$, in the experimentally accessible composition range, the $\text{CaAl}_{2-x}\text{Si}_x$ electronic bands are accurately described by a rigid-band model; in this range $g(\epsilon_F)$ monotonically increases with x , so that the measured non-monotonic variations in the superconducting properties cannot be associated with changes in the density of states at the Fermi level. These findings provide a useful reference and a strong motivation for a future, complete study of the electron-phonon interaction as a function of x .

The rigid-band model breaks down for $x < 0.6$, where the increasing aluminium content mainly leads to the emptying of the π bonding band, which finally drives the compound unstable. The occurrence of such a dynamical instability is related to an abrupt change in the c/a ratio and correlates with the persistence of the interlayer band at the Fermi level, related to the pinning of the C_d states. Therefore, although isostructural and isoelectronic with MgB_2 , the C_{32} phase of CaAl_2 is unstable and doesn't share strong similarities with its electronic bands.

The main result of this work is that the interlayer band, empty in MgB_2 , and the “out-of-plane” phonons (optical B_{1g} and acoustical A_{2u} at Γ), irrelevant for superconductivity in MgB_2 , play a major role on the stability and superconductivity of C_{32} intermetallic compounds, once the structural parameters c and a assume appropriate values. This observation goes beyond the CaAlSi family and represents the starting point for further studies of a wider class of hexagonal, graphite-like compounds.⁴³

VI. ACKNOWLEDGMENTS

We are very grateful to Ole K. Andersen for useful conversations and to Jens Kortus for a critical reading of this manuscript. One of us (GGB) gratefully acknowledges partial financial support from MIUR (the Italian Ministry for Education, University and Research) through COFIN2003.

- * Present Address: Unité de Physico-Chimie et de Physique des Matériaux, Université Catholique de Louvain, 1 place Croix du Sud, B-1348 Louvain-la-Neuve, Belgium
- ¹ J. Nagamatsu, N. Nakagawa, T. Muranaka, Y. Zenitani and J. Akimitsu. *Nature (London)*, **410**:63, (2001).
 - ² P. Villars and L.D. Calvert. *Pearson's Handbook of Crystallographic Data for Intermetallic Phases*, 2nd ed. ASM International, Materials Park, OH,, (1991).
 - ³ B. Lorenz, J. Lenzi, J. Cmaidalka, R. L. Meng, Y. Y. Sun, Y. Y. Xue and C. W. Chu. *Physica C*, **383**,191, (2002).
 - ⁴ B. Lorenz, J. Cmaidalka, R. L. Meng and C. W. Chu. *Phys. Rev. B*, **68**,14512, (2003).
 - ⁵ S. Kuroiea, H. Takagiwa, M. Yamazawa and J. Akimitsu. *cond-mat*, **0402483**, (2004).
 - ⁶ S. Tsuda, T. Yokoya, S. Shin, M. Imai, I. Hase. *Phys. Rev. B*, **69**, 100506, (2004).
 - ⁷ I.R. Shein, N.I. Medvedeva, A.L. Ivanovskii. *J. Phys.: Condens. Matter*, **15**, L541, (2003).
 - ⁸ I.I. Mazin, D.A. Papaconstantopoulos. *Phys. Rev. B*, **69**, 1805, (2004).
 - ⁹ G.Q. Huang, L.F. Chen, M. Liu, D.Y. Xing. *Phys. Rev. B*, **69**, 064509, (2004).
 - ¹⁰ G. Q. Huang, L. F. Chen, M. Liu and D. Y. Xing. *Phys. Rev. B*, **71**, 172506, (2005).
 - ¹¹ In reality, CaAl₂ crystallises in the so-called MgCu₂ Laves phase, and, when doped with Li or Mg, in the MgNi₂ and MgZn₂ phases.^{12,13,14}; while theoretical and experimental work exists on these transitions, the effect of Si doping is still unexplored.
 - ¹² H.Tanaka, H.Takeshita, N. Kuriyama, T. Sakai, I. Uehara, D. Noreus, A. Züttel, L. Schlapbach, and S.Suda. *IEA Task 12: Metal Hydrides and Carbon for Hydrogen Storage*, page 23, 2001.
 - ¹³ S. Amerioun, S. I. Simak, and U. Haussermann. *Inorg. Chem.*, **42**, 1467, (2003).
 - ¹⁴ S. Amerioun, T. Yokosawa, S. Livin, and U. Haussermann. *Inorg. Chem.*, **43**, 4751, (2004).
 - ¹⁵ C. Petrovic R.A. Ribeiro, S.L. Bud'ko and P.C. Canfield. *Physica C*, **384**, 227, (2003).
 - ¹⁶ W. Kohn and L. J. Sham. *Phys. Rev.*, **40**, A1133, (1965).
 - ¹⁷ P. Hohenberg and W. Kohn. *Phys. Rev.*, **136**, B864, (1964).
 - ¹⁸ S. Baroni, S. de Gironcoli, A. Dal Corso, and P. Giannozzi. *Rev. Mod. Phys.*, **73**, 515, (2001).
 - ¹⁹ The ABINIT code is a common project of the Université Catholique de Louvain, Corning Incorporated, and other contributors. URL <http://www.abinit.org>.
 - ²⁰ S. Baroni, A. Dal Corso, S. de Gironcoli, P. Giannozzi, C. Cavazzoni, G. Ballabio, S. Scandolo, G. Chiarotti, P. Focher, A. Pasquarello, et al. URL <http://www.pwscf.org>.
 - ²¹ N. Troullier, J. L. Martins. *Phys. Rev. B*, **43**, 1993, (1991).
 - ²² M. Fuchs, M. Scheffler. *Comput. Phys. Commun.*, **119**, 67, (1999). URL <http://www.fhi-berlin.mpg.de/th/fhi98md/fhi98PP/>.
 - ²³ J.P. Perdew, K. Burke and M. Ernzerhof. *Phys. Rev. Lett.*, **77**, 3865, (1996).
 - ²⁴ H.J. Monkhorst, J.D. Pack. *Phys. Rev. B*, **13**, 5188, (1976).
 - ²⁵ P.E. Blöchl, O. Jepsen, O. K. Andersen. *Phys. Rev. B*, **49**, 16223, (1994).
 - ²⁶ N. Marzari, D. Vanderbilt, A. De Vita, M. C. Payne. *Phys. Rev. Lett.*, **82**, 3296, (1999).
 - ²⁷ L. Nordheim. *Ann. Phys. Leipzig*, **9**, 607, (1931).
 - ²⁸ M. Imai, K. Nishida, T. Kimura and H. Abe. *Appl. Phys. Lett.*, **80**, 1019, (2001).
 - ²⁹ J. Kortus, I. I. Mazin, K. D. Belashchenko, V. P. Antropov, and L. L. Boyer. *Phys. Rev. Lett.*, **86**, 4656, (2001).
 - ³⁰ J. M. An and W. E. Pickett. *Phys. Rev. Lett.*, **86**, 4366, (2001).
 - ³¹ M. Posternak, A. Baldereschi, A. J. Freeman, E. Wimmer, and M. Weinert. *Phys. Rev. Lett.*, **50**, 761, (1983).
 - ³² M. Giantomassi. Elettroni, fononi e proprietà strutturali del composto CaAl_{2-x}Si_x, (2005). Master Thesis, unpublished.
 - ³³ Y. Kong, O. V. Dolgov, O. Jepsen, and O. K. Andersen. *Phys. Rev. B*, **64**, 020501, (2001).
 - ³⁴ G. Satta, G. Profeta, F. Bernardini, A. Continenza, and S. Massidda. *Phys. Rev. B*, **64**, 104507, (2001).
 - ³⁵ S. Piscanec, M. Lazzeri, Francesco Mauri, A. C. Ferrari, and J. Robertson. *Phys. Rev. Lett.*, **93**, 185503, (2004).
 - ³⁶ Frozen-phonon calculations, not shown, confirm that the interlayer intraband scattering is also negligible.
 - ³⁷ In some cases, when there is a clear experimental hint for the stability of a certain compound in a given structure, and when the instability is limited to a few **q**-points, it is possible to use a generalized approach to include the contribution of phonons with small, imaginary frequencies to the total electron-phonon coupling. We think that in our case this approach cannot be followed: here a whole branch has imaginary frequencies, which simply tells that our fictitious \square^{2+} AlSi is not stable.
 - ³⁸ In the MgCu₂ Laves phase (space group No. 227)² the Ca atoms sit on (8a) and Al on (16d) sites, with a lattice parameter of 8.04 Å. We checked that the total energy of CaAl₂, in the optimised Laves phase structure ($a = 8.06$ Å), is lower than in the AlB₂ structure by 0.2 eV/f.u.
 - ³⁹ In other words, this hypothetical C₃₂ is stable against lattice vibrations at fixed c and a , although obviously unstable against structural relaxation of c and a .
 - ⁴⁰ S. Fahy and D.R. Hamann. *Phys. Rev. B*, **41**, 7587, (1990).
 - ⁴¹ At P=16 GPa CaSi₂ crystallises in a slightly distorted C₃₂ phase⁴², which has been studied by Satta *et al.*³⁴.
 - ⁴² P. Bordet, M. Affronte, S. Sanfilippo, M. Nunez-Regueiro, O. Laborde, G. L. Olcese, and A. Palenzona. *Phys. Rev. B*, **62**, 11392, (2000).
 - ⁴³ L. Boeri, M. Giantomassi, G.B. Bachelet, and O.K. Andersen. *Unpublished*.